Journal of Engineering Mathematics 17 (1983) 285–300

A numerical solution of the vertical boundary-layer equations in a horizontally heated porous cavity

P.G. DANIELS

Department of Mathematics, The City University, Northampton Square, London, England EC1V 0HB

(Received March 1, 1983; in revised form June 3, 1983)

Summary

A numerical scheme for the solution of the vertical boundary-layer equations in a two-dimensional horizontally heated cavity filled with a porous medium is described. A novel feature of the problem is that although the equations are parabolic, the core boundary conditions at the edge of the layer are not specified *a priori*. Instead the core stream function and temperature profiles must satisfy certain symmetry conditions requiring an iterative approach in the numerical scheme. The results confirm the possibility of the frequently assumed hypothesis in cavity flows that the vertical boundary layers empty into the core and thus complete the main flux circulation in the cavity. The numerical results are compared with both asymptotic and approximate solutions of the equations.

1. Introduction

In a variety of high Rayleigh number cavity flows driven by horizontal heating, the vertical boundary layers play a key role in the completion of the circulation through the system. In the core region between the boundary layers the initial assumption of a constant temperature flow [1] was revised in the context of a magneto-hydrodynamic system by Singh and Cowling [2] and later in the case of a Newtonian fluid by Gill [3]. These studies developed the notion of a horizontally stratified core in which the flow is also horizontal. Above the mid-level of the cavity the fluid is detrained by the boundary layer on the hot wall, crosses to the vertical boundary layer on the cold wall where it descends and is returned to the hot wall by an equal and opposite flow in the lower half of the cavity. Provided the boundary conditions on the upper and lower surfaces of the cavity are the same (and the physical properties of the fluid are constant), it may be assumed that the solution of the system is "centro-symmetric" and the horizontal velocity and temperature profiles in the core can be found by consideration of the solution in just one of the vertical boundary layers. At the edge of the boundary layer the stream function and temperature profiles must possess appropriate properties of symmetry, but are not known *a priori*, being determined by the solution of the boundary-layer system, while at the ends of the layer it is generally assumed [2,3] that the stream function vanishes, so that the fluid rising or descending in the layer empties into the core, rendering the boundary layers on the horizontal walls relatively unimportant. These assumptions have led to various approximate solutions of the vertical boundary layer system. Singh and Cowling [2] used a Pohlhausen approach, while Gill [3] obtained approximate solutions in the Newtonian problem for the case of infinite Prandtl number by a modified Oseen method.

A similar method was used for the analogous problem in a porous medium by Weber [4], and more recently Blythe and Simpkins [5,6,7] have obtained approximate solutions to both the porous problem and the infinite Prandtl number Newtonian problem using an integral relations technique. Walker and Homsy [8] have also considered the porous problem and have obtained numerical solutions of the boundary-layer equations for various specified external temperature profiles using a trial and error method to determine a profile for which the resulting core stream function is symmetric.

In the absence, then, of any exact solution to the vertical boundary layer problem, the present study attempts to provide an "exact" numerical solution of the equations for the porous case in which the external temperature and stream function are obtained by an iterative technique. The convergence of the scheme appears to confirm the possibility of a solution in which the layer empties into the core, and also provides a comparison with the asymptotic structure of the solution at the ends of the layer, recently studied by Blythe, Daniels and Simpkins [9]. A correct analysis of this structure is vitally important for the consideration of the boundary layers on the horizontal walls, an investigation of which appears to be the only means of testing the validity of the conditions applied at the ends of the vertical layers.

The governing equations and boundary conditions are stated in Section 2, along with the pertinent features of their asymptotic structure. This system is discretized using finite differences, and the parabolic equations are then solved by marching in the direction of forward flow in the layer; the final external temperature and stream function profiles are determined by an iterative technique which necessitates several sweeps of the layer. Details of the scheme are described in Section 3, and the results are compared with the asymptotic solutions of the equations in Section 4.

2. Governing equations and asymptotic properties

A steady convective roll is set up within a two-dimensional, porous, rectangular cavity of height h and width l by maintaining the vertical boundaries at different constant temperatures, T_0 and T_1 ($T_0 < T_1$). The Boussinesq equations governing the motion may be written in the form (see, for example, [7])

$$\frac{\partial \bar{u}}{\partial \bar{x}} + \frac{\partial \bar{w}}{\partial \bar{z}} = 0, \tag{2.1}$$

$$\frac{\partial \bar{w}}{\partial \bar{x}} - \frac{\partial \bar{u}}{\partial \bar{z}} = R\frac{\partial \bar{T}}{\partial \bar{x}}, \tag{2.2}$$

$$\nabla^2 \bar{T} = \bar{u}\frac{\partial \bar{T}}{\partial \bar{x}} + \bar{w}\frac{\partial \bar{T}}{\partial \bar{z}}, \tag{2.3}$$

where

$$\nabla^2 = \frac{\partial^2}{\partial \bar{x}^2} + \frac{\partial^2}{\partial \bar{z}^2}, \tag{2.4}$$

$(\bar{x}, \bar{z})$ are Cartesian co-ordinates non-dimensionalized with respect to the height of the

cavity, with origin at the base of the cold wall and $(\bar{u}, \bar{w})$ are corresponding velocity components non-dimensionalized with respect to κ/h where κ is the thermal diffusivity. $\bar{T}$ is the non-dimensional temperature in excess of T_0, scaled with respect to $T_1 - T_0$. The two parameters of the problem are the aspect ratio, L, and the Darcy-Rayleigh number, R, defined by

$$L = \frac{l}{h}, \qquad R = \frac{k_p \alpha g h (T_1 - T_0)}{\kappa \nu}, \tag{2.5}$$

where k_p is the permeability, α is the coefficient of thermal expansion, g is the acceleration due to gravity and ν is the kinematic viscosity. The present study is concerned with the solution at large Rayleigh numbers and finite values of L; multiple-cell solutions of the type found in large and small aspect ratio cavities are not considered.

Appropriate boundary conditions on the vertical walls at $\bar{x} = 0$ and $\bar{x} = L$ are

$$\bar{u} = \bar{T} = 0 \qquad (\bar{x} = 0), \tag{2.6}$$

$$\bar{u} = 0, \ \bar{T} = 1 \qquad (\bar{x} = L), \tag{2.7}$$

and provided suitable conditions are chosen on the horizontal walls at $z = 0$ and $z = 1$, the equations and boundary conditions possess the centro-symmetric properties

$$\bar{\psi}(\bar{x}, \bar{z}) = \bar{\psi}(L - \bar{x}, 1 - \bar{z}), \tag{2.8}$$

$$\bar{T}(\bar{x}, \bar{z}) = 1 - \bar{T}(L - \bar{x}, 1 - \bar{z}), \tag{2.9}$$

where $\bar{\psi}$ is the stream function defined by $\bar{u} = \partial\bar{\psi}/\partial\bar{z}$, $\bar{w} = -\partial\bar{\psi}/\partial\bar{x}$.

For large values of the Darcy-Rayleigh number, the solution consists of a parallel stratified shear flow

$$\bar{\psi} = R^{1/2}\psi_c(\bar{z}) + \ldots, \qquad \bar{T} = T_c(\bar{z}) + \ldots \quad (R \gg 1) \tag{2.10}$$

between boundary layers of thickness $O(R^{-1/2})$ on each vertical wall. Near the cold wall $\bar{x} = 0$ we write

$$\bar{\psi} = R^{1/2}\psi(x, z) + \ldots, \qquad \bar{T} = T(x, z) + \ldots,$$

$$\bar{x} = R^{-1/2}x, \qquad \bar{z} = z, \tag{2.11}$$

to obtain the boundary-layer system

$$\frac{\partial u}{\partial x} + \frac{\partial w}{\partial z} = 0, \qquad \frac{\partial w}{\partial x} = \frac{\partial T}{\partial x}, \qquad u\frac{\partial T}{\partial x} + w\frac{\partial T}{\partial z} = \frac{\partial^2 T}{\partial x^2}$$

$$(0 < z < 1, \quad x > 0) \tag{2.12}$$

where $u = \partial\psi/\partial z$, $w = -\partial\psi/\partial x$. At the wall the boundary conditions are

$$u = T = 0 \quad (x = 0) \tag{2.13}$$

while at the edge of the layer we require that the solution matches with that (2.10) in the core

$$\psi \to \psi_c(z), \qquad T \to T_c(z) \quad (x \to \infty), \tag{2.14}$$

where ψ_c and T_c, in view of the centro-symmetry relations (2.8), (2.9), must satisfy

$$\psi_c(z) = \psi_c(1-z), \qquad T_c(z) = 1 - T_c(1-z). \tag{2.15}$$

Conditions at the ends of the layer are taken to be

$$\psi(x, 0) = \psi(x, 1) = 0. \tag{2.16}$$

In the present paper we consider the numerical solution of the system (2.12)–(2.16). Asymptotic solutions at each end of the layer, consistent with (2.16), have been determined by Blythe, Daniels and Simpkins [9], and as $z \to 1$ it is found that

$$\begin{aligned} &\psi = (1-z)^{1/2} f(\xi) + O(1-z), \\ &T = g(\xi) + O\big((1-z)^{1/2}\big), \quad (z \to 1-), \end{aligned} \tag{2.17}$$

where $\xi = x/(1-z)^{1/2}$, $g = 1 - f'$ and f satisfies

$$f''' + \tfrac{1}{2} f f'' = 0, \qquad f(0) = 0, \qquad f'(0) = 1, \qquad f'(\infty) = 0. \tag{2.18}$$

The solution of this system has been determined in different contexts by Sakiadis [10], Howarth [11] and Singh and Cowling [12], and has the property

$$f(\infty) = a = 1.616\ldots \tag{2.19}$$

so that

$$\psi_c \sim a(1-z)^{1/2}, \qquad T_c \sim 1 - O\big((1-z)^{1/2}\big), \quad (z \to 1-). \tag{2.20}$$

The form of ψ_c near $z = 1$ and the symmetry conditions (2.15) dictate the structure of the solution near $z = 0$, where it is found (Blythe, Daniels and Simpkins [9]) that solutions of the form

$$\begin{aligned} &\psi \sim z^{1/2} a\left(1 - \exp\left(-\frac{\beta x}{a}\right)\right) + \ldots, \\ &T \sim z^{1/2} \beta\left(1 - \exp\left(-\frac{\beta x}{a}\right)\right) + \ldots, \end{aligned} \qquad (z \to 0+,\ 0 < x < \infty), \tag{2.21}$$

are uniformly valid to leading order across the layer, although higher-order terms are modified within an inner thermal layer of thickness $x = O(z^{1/4})$. The value of the constant β remains undetermined by the asymptotic analysis, although the higher-order corrections to the core temperature profile near $z = 0$ may be determined in terms of β:

$$T_c \sim \beta z^{1/2} + 1.443 \beta^{4/3} z^{2/3} + O(z^{7/9}), \quad (z \to 0). \tag{2.22}$$

The leading term generates the first correction to the solution (2.17) near $z = 1$ via the symmetry conditions (2.15), which also imply that

$$\psi_c \sim az^{1/2} + O(z), \quad (z \to 0). \tag{2.23}$$

3. Discretization

For the purpose of discretization, it is convenient to recast the system (2.12)–(2.16) using the transformations

$$x = \frac{1}{\sqrt{2}} X, \qquad z = \tfrac{1}{2}(2 - Z), \qquad \psi(x, z) = \frac{1}{\sqrt{2}} \Phi(Z, X), \qquad T(x, z) = \theta(Z, X), \tag{3.1}$$

to obtain the fundamental problem

$$\frac{\partial^2 \Phi}{\partial X^2} = -\frac{\partial \theta}{\partial X}, \qquad \frac{\partial \Phi}{\partial X}\frac{\partial \theta}{\partial Z} - \frac{\partial \Phi}{\partial Z}\frac{\partial \theta}{\partial X} = \frac{\partial^2 \theta}{\partial X^2}, \tag{3.2}$$

$$\Phi = \theta = 0 \quad (X = 0), \tag{3.3}$$

$$\Phi \to \Phi_c(Z), \qquad \theta \to \theta_c(Z) \quad (X \to \infty), \tag{3.4}$$

where

$$\Phi_c(Z) = \Phi_c(2 - Z), \qquad \theta_c(Z) = 1 - \theta_c(2 - Z) \tag{3.5}$$

and

$$\Phi(0, X) = \Phi(2, X) = 0. \tag{3.6}$$

The entire layer $0 < Z < 2$, $X > 0$ is now divided into two parts, $0 < Z < 1$ (region I) and $1 < Z < 2$ (region II) and a different discretization is used in each region.

In region I we must cater for the initial development in the similarity form (2.17) and so we write

$$\begin{aligned} &\Phi = \zeta A(\zeta, \eta), \qquad \Phi_c = \zeta A_c(\zeta), \\ &\theta = B(\zeta, \eta), \qquad \theta_c = B_c(\zeta) \end{aligned} \tag{3.7}$$

where

$$\zeta = Z^{1/2}, \qquad \eta = X/Z^{1/2}. \tag{3.8}$$

We also define

$$C = \frac{\partial A}{\partial \eta}, \qquad D = \frac{\partial B}{\partial \eta}. \tag{3.9}$$

We shall assume that for $Z < 1$, $\theta_c(Z)$ is a known function so that the equations (3.2) may now be written in the form

$$B = B_c - C, \tag{3.10}$$

$$\frac{\partial D}{\partial \eta} = \tfrac{1}{2}\zeta C\frac{\partial B}{\partial \zeta} - \tfrac{1}{2}D\left(A + \zeta\frac{\partial A}{\partial \zeta}\right). \tag{3.11}$$

The initial conditions at $\zeta = 0$ are

$$A(0,\eta) = f(\eta), \qquad C(0,\eta) = f'(\eta), \qquad B(0,\eta) = g(\eta), \qquad D(0,\eta) = g'(\eta), \tag{3.12}$$

where f and g are defined by (2.17) and (2.18).

The set of equations (3.9–3.11) now contains only first derivatives and is discretized in the domain $0 \leqslant \eta \leqslant \eta_I$, $0 \leqslant \zeta \leqslant 1$ using central differences in both the η and ζ directions to obtain

$$\begin{aligned}
&A_{i+1} - A_i - \frac{h}{2}(C_i + C_{i+1}) = 0 && (i = 0, 1, \ldots I-1),\\
&B_{i+1} - B_i - \frac{h}{2}(D_i + D_{i+1}) = 0 &&\\
&B_i + C_i - B_c = 0 && (i = 0, 1, \ldots I),\\
&D_{i+1} + \bar{D}_{i+1} - D_i - \bar{D}_i - \frac{h}{32k}\{(\zeta + \bar{\zeta})(C_i + \bar{C}_i + C_{i+1} - \bar{C}_{i+1})\\
&\quad \times (B_i + B_{i+1} - \bar{B}_i - \bar{B}_{i+1}) - (D_i + \bar{D}_i + D_{i+1} + \bar{D}_{i+1})\\
&\quad \times [(A_i + A_{i+1})(k + \zeta + \bar{\zeta}) + (\bar{A}_i + \bar{A}_{i+1})(k - \zeta - \bar{\zeta})]\} = 0
\end{aligned} \tag{3.13}$$

Equations (3.9) and (3.10) are centred on the current mesh values (ζ, η_i) while (3.11) is centred between these and the previous mesh values $(\bar{\zeta}, \eta_i)$; function values at the latter points are assumed known and denoted by an overbar. The step lengths in the ζ and η directions are k and h respectively, with $\zeta = \bar{\zeta} + k$, $\eta_{i+1} = \eta_i + h$. The boundary conditions (3.3), (3.4) become

$$A_0 = B_0 = 0, \qquad B_I = B_c \tag{3.14}$$

so that (3.13), (3.14) consist of $4(I+1)$ equations for the $4(I+1)$ unknowns A_i, B_i, C_i, D_i $(i = 0, \ldots I)$. Newton iteration is used to find the solution at each ζ step, providing a linear matrix equation for the corrections to the previous estimate of the solution, the initial guess being taken as the solution at the previous ζ step. The matrix is of dimension $4(I+1) \times 4(I+1)$ but may be arranged in a form in which there are just four non-zero diagonals either side of the main diagonal and is easily solved by a standard Gaussian elimination for a banded system.

The solution in the first half of the layer may now be computed forward from the initial profile (3.12) to the centre of the layer $Z = 1$, provided that the external temperature field $\theta_c(Z)$, $(Z < 1)$, is supplied. This is guessed initially and region I solved to obtain a corresponding stream function $\Phi_c(Z) = \zeta A_c(\zeta)$. The symmetry condition (3.5) requires that $\Phi_c(2 - Z) = \Phi_c(Z)$ so that in region II we follow an inverse procedure, specifying the symmetric continuation of the core stream function and obtaining a temperature profile $\theta_c(Z)$, $(Z > 1)$.

This procedure suggests the following discretization in region II:

$$\begin{aligned} \Phi &= \tilde{\zeta}\tilde{A}(\tilde{\zeta}, X), \qquad \Phi_c = \tilde{\zeta}\tilde{A}_c(\tilde{\zeta}), \\ \theta &= \tilde{B}(\tilde{\zeta}, X), \qquad \theta_c = \tilde{B}_c(\tilde{\zeta}) \end{aligned} \tag{3.15}$$

where

$$\tilde{\zeta} = (2 - Z)^{1/2} \quad (0 \leqslant \tilde{\zeta} \leqslant 1), \tag{3.16}$$

and we specify

$$\tilde{A}_c(\tilde{\zeta}) = A_c(\tilde{\zeta}), \quad (0 \leqslant \tilde{\zeta} \leqslant 1). \tag{3.17}$$

Note that the transformation (3.16) is necessary since A_c is known only at mesh values of ζ in (3.17) which now correspond to appropriate mesh values of $\tilde{\zeta}$. However, the lateral co-ordinate is now taken as X in view of the asymptotic form (2.21), which also suggests that $\tilde{B}$ should be a linear function of $\tilde{\zeta}$ as $\tilde{\zeta} \to 0$. We define

$$\tilde{C} = \frac{\partial \tilde{A}}{\partial X}, \qquad \tilde{D} = \frac{\partial \tilde{B}}{\partial X} \tag{3.18}$$

and equations (3.2) become

$$\tilde{D} = -\tilde{\zeta}\frac{\partial \tilde{C}}{\partial X}, \tag{3.19}$$

$$\tilde{\zeta}\frac{\partial \tilde{D}}{\partial X} = -\tfrac{1}{2}\tilde{\zeta}\tilde{C}\frac{\partial \tilde{B}}{\partial \tilde{\zeta}} + \tfrac{1}{2}\tilde{D}\left(\tilde{A} + \tilde{\zeta}\frac{\partial \tilde{A}}{\partial \tilde{\zeta}}\right). \tag{3.20}$$

These are again of first-order and are discretized using central differences in both the $\tilde{\zeta}$ and X directions. The external boundary conditions are taken as

$$\tilde{A} \to \tilde{A}_c(\tilde{\zeta}), \qquad \tilde{D} \to 0 \quad (X \to \infty), \tag{3.21}$$

the extra condition being required since the unintegrated form (3.19) of the momentum equation is used, the core temperature profile now being unknown but allowed to depend on $\tilde{\zeta}$ by the second condition in (3.21). Solutions were also computed with this condition replaced by $\tilde{C} \to 0$ as $X \to \infty$ but this was found to have an insignificant effect on the results. The wall conditions are

$$\tilde{A}(\tilde{\zeta}, 0) = \tilde{B}(\tilde{\zeta}, 0) = 0 \tag{3.22}$$

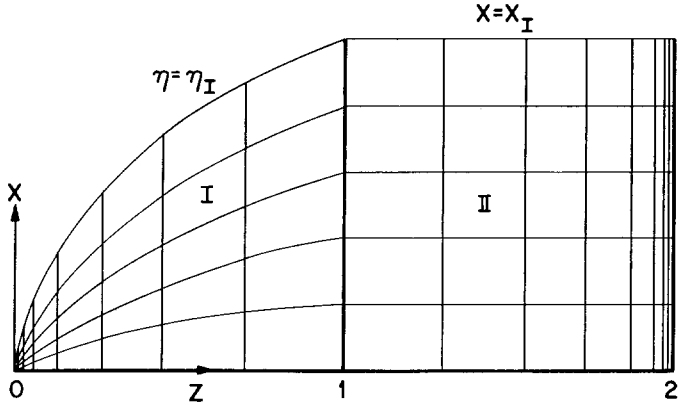

Figure 1. Schematic diagram of the mesh pattern in the Z, X plane.

and the initial conditions at $\tilde{\zeta} = 1$ are

$$\tilde{A}(1, X) = A(1, X), \qquad \tilde{B}(1, X) = B(1, X),$$

$$\tilde{C}(1, X) = C(1, X), \qquad \tilde{D}(1, X) = D(1, X). \tag{3.23}$$

Here the switch between the two meshes is made particularly simple by use of the streamwise variable Z. At $Z = 1$, we have $\eta = X/Z^{1/2} = X$ so that the mesh points across the layer in region I automatically coincide with equally spaced points in X across region II (see Fig. 1). The step length in $\tilde{\zeta}$ must be taken as k. The discretization of (3.17)–(3.23) is now completed in a similar fashion to that of region I to obtain $4(I + 1)$ equations for the $4(I + 1)$ unknowns $\tilde{A}_i$, $\tilde{B}_i$, $\tilde{C}_i$, $\tilde{D}_i$ $(i = 0, \ldots I)$ at each $\tilde{\zeta}$ step (the extra boundary condition in (3.21) replaces the equation in (3.13) corresponding to the value $i = I$, which is now inadmissible in (3.19)). The Newton iteration may again be reduced to the solution of a nine-band matrix of dimension $4(I + 1) \times 4(I + 1)$.

The solution is now computed from $\tilde{\zeta} = 1$ to $\tilde{\zeta} = 0$ and determines the external temperature profile

$$\theta_c(Z) = \tilde{B}_I = \tilde{B}_c(\tilde{\zeta}) \quad (1 < Z < 2). \tag{3.24}$$

Since $A_c(0) = 0$ it follows from (3.17) that $\tilde{A}_c(\tilde{\zeta}) \to 0$ as $\tilde{\zeta} \to 0$ and this automatically ensures that $\tilde{B}_c(\tilde{\zeta}) \to 0$ as $\tilde{\zeta} \to 0$.

The solution so computed does not generally satisfy the final constraint on the problem, which requires that the external temperature field satisfies the anti-symmetry condition

$$B_c(\zeta) = 1 - \tilde{B}_c(\zeta) \quad (0 \leqslant \zeta \leqslant 1). \tag{3.25}$$

This is achieved by applying the iterative procedure

$$B_c(\zeta) = rB_c(\zeta) + (1 - r)\big(1 - \tilde{B}_c(\zeta)\big), \quad (0 \leqslant \zeta \leqslant 1), \tag{3.26}$$

to obtain a new estimate for the core temperature field in the first half of the layer. The

profiles B_c and $\tilde{B}_c$ on the right hand side of (3.26) are the values pertaining to the previous sweep of the layer, and r is introduced as a relaxation factor.

4. Numerical results

Before implementing the iterative scheme, the program was checked by applying the external temperature profile $\theta_c = 1$ for all $0 < Z < 2$, replacing the conditions (3.21) in region II by $\tilde{B} \to 1$ and $\tilde{C} \to 0$ as $X \to \infty$. Step sizes of $h = 0.2$, $k = 0.02$ and an outer boundary at $\eta_I = 20$ and $X_I = 20$ were used, and on each downstream step the Newton iteration was required to converge to within a tolerance of 10^{-7}. The similarity solution was successfully reproduced, the solution in region I remaining effectively unaltered from the initial profile, and in region II values of the stream function and temperature being given accurately to at least three decimal places. A second test run was performed using a different external temperature profile, $\theta_c = 1 - \frac{1}{2}Z^{1/2}$, $(Z < 1)$, $\theta_c = \frac{1}{2}(2 - Z)^{1/2}$, $(Z > 1)$, and this generated an asymmetric stream function profile, as in the numerical experiments of Walker and Homsy [8].

The iterative scheme was now implemented, using the same external temperature profile in $Z < 1$:

$$B_c = 1 - \tfrac{1}{2}\zeta \quad (0 \leqslant \zeta \leqslant 1), \tag{4.1}$$

and a relaxation factor of $r = 0.3$. The resulting core stream function in $0 < Z < 1$ is shown by the broken curve in Fig. 2. The symmetric continuation of this is now imposed in region II and generates the core temperature profile also shown by a broken curve in Fig. 2. The correction feeds back into the system in region I via the iterative relation (3.26). After just one additional sweep of the layer, both Φ_c and θ_c are sufficiently close to the final profiles shown by the continuous (heavy) curves in Fig. 2 as to be almost indistinguishable on the scale of the drawing. Details of the convergence rates are given in Table 1. The iterative scheme was in fact continued until the temperature profile satisfied

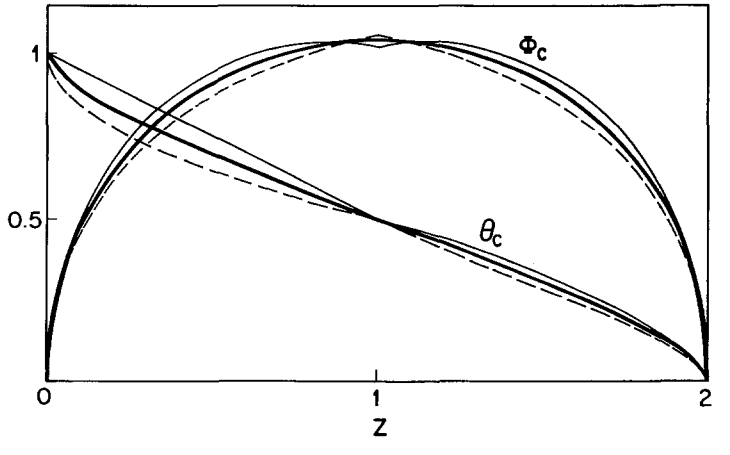

Figure 2. The first sweep of the layer for initial profiles: (i) $\theta_c = 1 - \frac{1}{2}Z^{1/2}$ $(Z < 1)$ (broken lines), and (ii) $\theta_c = 1 - \frac{1}{2}Z$ $(Z < 1)$ (unbroken lines), showing the stream function and temperature profiles Φ_c and θ_c. The final converged state (heavy lines) is also shown.

Table 1
Convergence properties for a solution with $r = 0.3$, $h = 0.2$, $k = 0.02$, $\eta_I = X_I = 20$ and the initial profile (4.1)

Iteration	$A_c(1)$	$D_0(1)$	$A_c(0.8)$	$B_c(0.8)$	$D_0(0.8)$	$A_c(0.5)$	$B_c(0.5)$	$D_0(0.5)$	$A_c(0.2)$	$B_c(0.2)$	$D_0(0.2)$
0	1.057	0.1720	0.9478	0.6000	0.2202	0.6796	0.7500	0.2986	0.3036	0.9000	0.3837
1	1.041	0.1756	0.9800	0.6396	0.2422	0.7046	0.7982	0.3260	0.3091	0.9279	0.4004
2	1.041	0.1754	0.9753	0.6367	0.2413	0.7072	0.8043	0.3298	0.3104	0.9344	0.4044
3	1.040	0.1756	0.9759	0.6375	0.2417	0.7077	0.8056	0.3307	0.3107	0.9362	0.4055
4	1.040	0.1755	0.9757	0.6374	0.2417	0.7078	0.8058	0.3308	0.3108	0.9367	0.4058
5	1.040	0.1755	0.9757	0.6375	0.2417	0.7078	0.8058	0.3308	0.3108	0.9368	0.4058
6	1.040	0.1755	0.9757	0.6375	0.2417	0.7078	0.8059	0.3308	0.3108	0.9368	0.4059
7	1.040	0.1755	0.9757	0.6375	0.2417	0.7078	0.8059	0.3308	0.3108	0.9368	0.4059

Table 2
Results for varying step-sizes and outer boundaries compared with previous approximate solutions

h	k	η_I	X_I	$\psi_c(\frac{1}{2})$	$T_c'(\frac{1}{2})$
0.1	0.02	30	30	0.73536	0.7515
0.2	0.02	30	30	0.73564	0.7518
0.2	0.01	30	30	0.73562	0.7521
0.2	0.02	20	20	0.73562	0.7522
0.2	0.01	30	50	0.73562	0.7523
Walker and Homsy [8]				0.733	0.75
Weber [4]				0.87	0.67
Simpkins and Blythe [7] (profile (c))				0.734	0.726

the condition of anti-symmetry to within a tolerance of 10^{-6}. This was achieved in ten iterations. The Newton iteration on each downstream step typically required between three and five solutions of the matrix equation. The gradients $d\Phi_c/dZ$ and $d\theta_c/dZ$ automatically become continuous at the mid-point $Z = 1$ as the system converges.

Various tests were made to investigate both the convergence and accuracy of the scheme and some of the results are summarized in Table 2. The rate of convergence was fairly insensitive to the value of the relaxation factor and although values of $r = 0.2$ and $r = 0.5$ were tested, the original value of 0.3 appeared to be slightly preferable. Provided the initial temperature profile satisfies $\theta_c(1) = \frac{1}{2}$, (3.26) implies that subsequent profiles also satisfy this condition. The linear form $B_c = 1 - \frac{1}{2}Z = 1 - \frac{1}{2}\zeta^2$ was also used as an initial profile in $0 \leqslant \zeta \leqslant 1$, the first sweep of the layer producing the continuous (light) curves shown in Fig. 2 with convergence following equally rapidly.

The final results are summarized, in terms of the original variables $\psi(x, z)$ and $T(x, z)$, in Table 3 and Figs. 3–5. For most runs the outer boundary was taken at $\eta_I = X_I = 30$, the relatively large value being required because the layer thickens appreciably as the fluid approaches, and turns, the corner at $Z = 2$. Although the asymptotic result (2.21) shows that the thickness of the layer is finite at $Z = 2$, the scale of decay is $x \sim a\beta^{-1}$ and it emerges that β is small. In order to achieve a good comparison with the asymptotic results, and to determine the unknown constant β, a run was made with $k = 0.01$, $h = 0.2$ and an

Table 3
Final values of the core stream function and temperature extrapolated from the numerical results

ζ	ψ_c	T_c
0	0	1
0.1	0.112	0.972
0.2	0.220	0.937
0.3	0.321	0.897
0.4	0.415	0.854
0.5	0.500	0.806
0.6	0.576	0.754
0.7	0.640	0.698
0.8	0.690	0.637
0.9	0.723	0.572
1	0.735	0.5

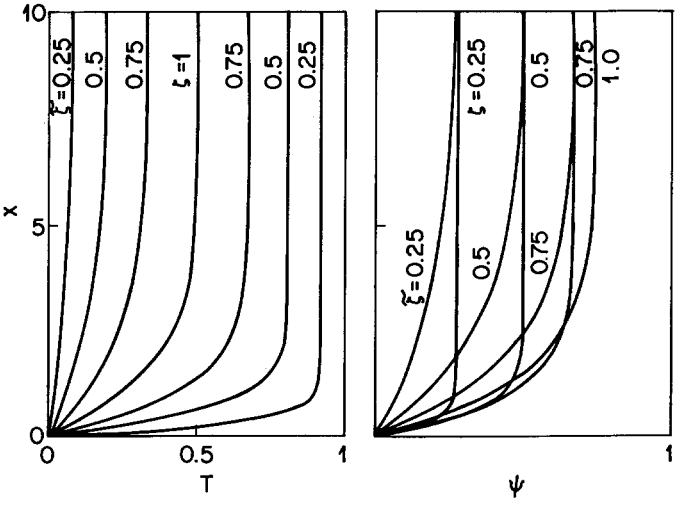

Figure 3. Temperature and stream function profiles across the layer at various values of ζ and $\tilde{\zeta}$.

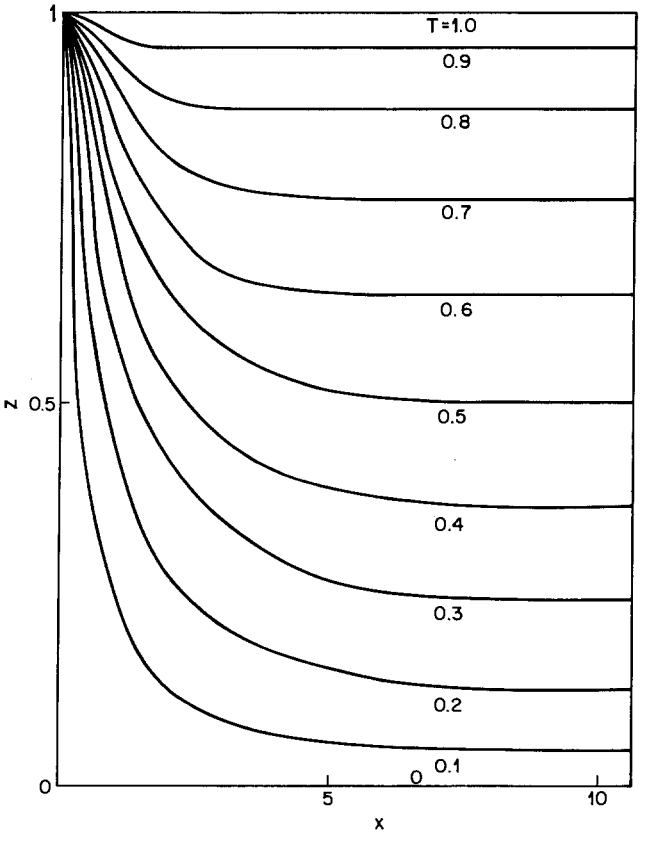

Figure 4. Isotherms in the boundary layer at intervals of 0.1.

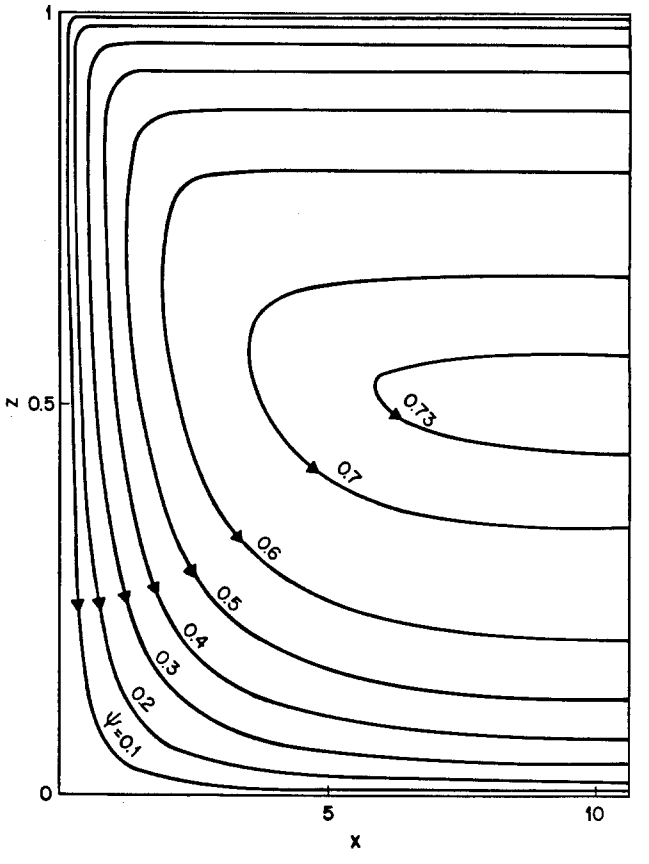

Figure 5. Streamlines in the boundary layer at intervals of 0.1.

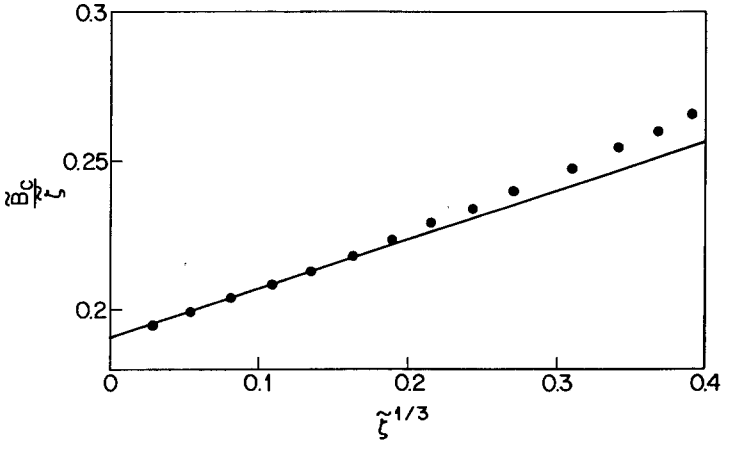

Figure 6. Comparison of the computed solution for the core temperature profile $\tilde{B}_c$ approaching $\tilde{\zeta} = 0$ (dots) and the asymptotic formula (4.2).

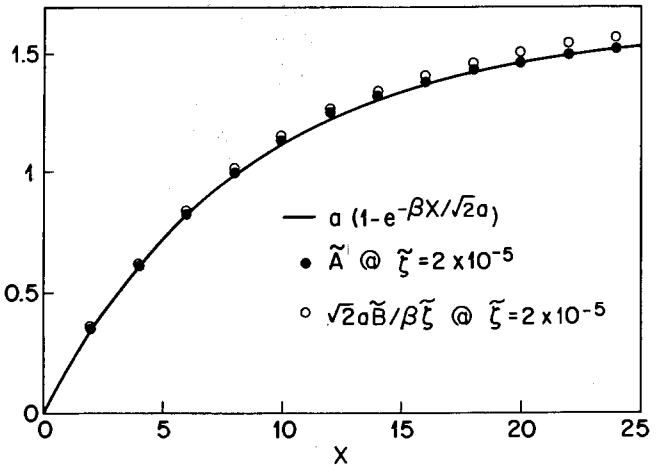

Figure 7. Comparison of the computed stream function (●) and temperature (○) profiles across the layer at $\tilde{\zeta} = 2\times 10^{-5}$, and the asymptotic formulae (2.21) with $\beta/\sqrt{2} = 0.191$ and $a = 1.616$.

outer boundary in region II at $X_I = 50$. In addition, much smaller step-sizes in the ζ and $\tilde{\zeta}$ directions were taken near $\zeta = 0$ and $\tilde{\zeta} = 0$, leading to the results shown in Figs. 6 and 7. From (2.22) we expect that as $\tilde{\zeta} \to 0$,

$$\tilde{B}_c \sim \frac{\beta}{\sqrt{2}}\tilde{\zeta} + 1.443\left(\frac{\beta}{\sqrt{2}}\right)^{4/3}\tilde{\zeta}^{4/3} + \ldots. \tag{4.2}$$

From Fig. 6 it is estimated that

$$\frac{\beta}{\sqrt{2}} = 0.19(1). \tag{4.3}$$

With $\beta/\sqrt{2} = 0.191$, the coefficient of the second term in (4.2) is 0.159 which should be compared with the value 0.166 obtained from the numerical solution, i.e. the gradient of the line in Fig. 6. The influence of the higher-order terms in (4.2) can also be seen from Fig. 6. The stream function and temperature profiles across the layer at the penultimate value of $\tilde{\zeta}$ are consistent with (4.3) and the exponential profile (2.21) (see Fig. 7).

5. Discussion

A comparison of the core profiles with the results of the various approximate methods is shown in Fig. 8. The agreement with the previous numerical solution of Walker and Homsy [8] is good throughout most of the layer, except near the ends at $z = 1$ and $z = 0$ where the form of the external profile assumed by Walker and Homsy explicitly excludes the correct asymptotic behavior (2.21). The main advantage of the present method is that the correct solution can be obtained to extremely good accuracy in just one or two sweeps of the layer. This is partly because the core temperature profile is known to satisfy $T_c(1) = 1$ and $T_c(\frac{1}{2}) = \frac{1}{2}$ and so a reasonable initial estimate of its form in $\frac{1}{2} < z < 1$ can be

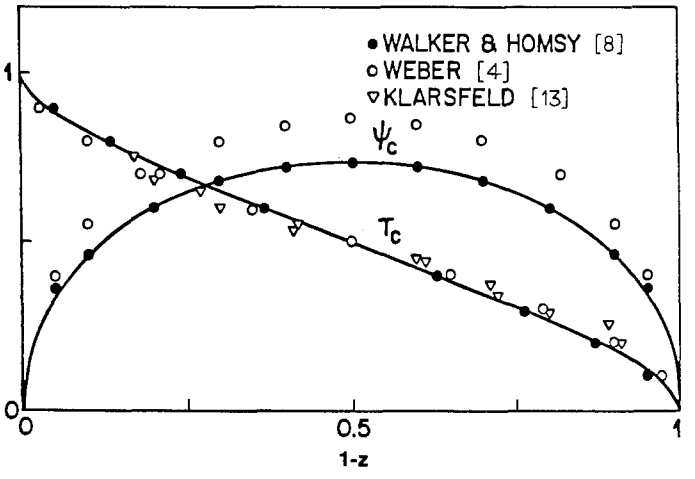

Figure 8. Comparison of the computed core stream function and temperature profiles with previous approximate solutions and the experimental results of Klarsfeld [13].

made. However, the success of the method is probably due to the way in which the scheme of iteration reflects the asymptotic composition of the layer. At the hot end, the flow, and the asymptotic solution (2.17), is forced by the external temperature field $T_c \sim 1$. This generates a core stream function $\psi_c = O((1-z)^{1/2})$ which, via the symmetry relations (2.15), generates the temperature field, and the asymptotic solution (2.21), at the cold end. In essence, the same procedure is followed in the numerical scheme.

The main result of the present work is the determination of the boundary-layer constant β in (4.3) since it seems unlikely that previous approximate theories, or the numerical approach of Walker and Homsy [8], can provide an accurate estimate of its value. The importance of the value of the constant β is that it plays a crucial role in the determination of the thickness of the boundary layers on the horizontal walls of the cavity. Indeed, it emerges [14,15] that the width of these layers is such as to have a considerable influence on the range of validity of the overall boundary-layer structure in the cavity at high Rayleigh numbers.

Finally, the heat transfer characteristics of the cavity are usually expressed in terms of a Nusselt number

$$\mathrm{Nu} = \int_0^1 \left.\frac{\partial \bar{T}}{\partial \bar{x}}\right|_{\bar{x}=0} \mathrm{d}\bar{z} \sim R^{1/2} \int_0^1 \left.\frac{\partial T}{\partial x}\right|_{x=0} \mathrm{d}z \tag{5.1}$$

which from the numerical solution is calculated to be

$$\mathrm{Nu} \sim R^{1/2} 0.51(5), \quad (R \gg 1). \tag{5.2}$$

Acknowledgements

The calculations were performed on the CDC 7600 computer of London University and the Cray-1 of Bell Laboratories, Murray Hill. The author is grateful to Dr. P.G. Simpkins

and Dr. P.A. Blythe for useful discussions and encouragement, and to Bell Laboratories for support during the course of this work.

References

[1] G.K. Batchelor, Heat transfer by free convection across a closed cavity between vertical boundaries at different temperatures. *Quart. Appl. Math.* 12 (1954) 209–233.

[2] K.R. Singh and T.G. Cowling, Thermal convection in magnetohydrodynamics, II: Flow in a rectangular box. *Quart. J. Mech. Appl. Math.* 16 (1963) 17–31.

[3] A.E. Gill, The boundary layer regime for convection in a rectangular cavity. *J. Fluid Mech.* 26 (1966) 515–536.

[4] J.E. Weber, The boundary layer regime for convection in a vertical porous layer. *Int. J. Heat Mass Transfer* 18 (1975) 569–573.

[5] P.A. Blythe and P.G. Simpkins, Thermal convection in a rectangular cavity. *Physico-chemical Hydrodynamics* 2 (1977) 511–524.

[6] P.A. Blythe and P.G. Simpkins, Convection in a porous layer for a temperature dependent viscosity. *Int. J. Heat Mass Transfer* 24 (1980) 497–506.

[7] P.G. Simpkins and P.A. Blythe, Convection in a porous layer. *Int. J. Heat Mass Transfer* 23 (1980) 881–887.

[8] K.L. Walker and G.M. Homsy, Convection in a porous cavity. *J. Fluid Mech.* 87 (1978) 449–474.

[9] P.A. Blythe, P.G. Daniels and P.G. Simpkins, Thermally driven cavity flows in porous media, I: The vertical boundary layer structure near the corners. *Proc. Roy. Soc.* A380 (1982) 119–136.

[10] B.C. Sakiadis, Boundary layer behaviour on continuous solid surfaces II: The boundary layer on a continuous flat surface. *A. I. Ch. Eng.* 7 (1961) 221–225.

[11] L.A. Howarth, Appendix to paper by Sir. G. Taylor, The dynamics of thin sheets of fluid, I. *Proc. Roy. Soc.* A253 (1959) 289–295.

[12] K.R. Singh and T.G. Cowling, Thermal convection in magnetohydrodynamics, I: Boundary layer flow up a hot vertical plate. *Quart. J. Mech. Appl. Math.* 16 (1963) 1–15.

[13] S. Klarsfeld, Champs de temperature associes aux movements de convection naturelle dans un milieu poreux limite. *Rev. Gen. Thermique* 9 (1970) 1403–1423.

[14] P.G. Daniels, P.A. Blythe and P.G. Simpkins, Thermally driven cavity flows in porous media, II: The horizontal boundary layer structure. *Proc. Roy. Soc.* A382 (1982) 135–154.

[15] P.A. Blythe, P.G. Simpkins and P.G. Daniels, Thermal convection in a cavity filled with a porous medium: a classification of limiting behaviours. *Int. J. Heat Mass Transfer* 26 (1983) 701–708.